JCTC Journal of Chemical Theory and Computation

ARTICLE

pubs.acs.org/JCTC

# Density Functional Restricted−Unrestricted/Molecular Mechanics Theory for Hyperfine Coupling Constants of Molecules in Solution

Zilvinas Rinkevicius,*[,†,∥] N. Arul Murugan,[†] Jacob Kongsted,[‡] Bogdan Frecuş,[†] Arnfinn Hykkerud Steindal,[§] and Hans Ågren[†]

[†]Department of Theoretical Chemistry & Biology, School of Biotechnology, Royal Institute of Technology, SE-106 91 Stockholm, Sweden

[‡]Department of Physics and Chemistry, University of Southern Denmark, Campusvej 55, DK-5230 Odense M, Denmark

[§]Centre of Theoretical and Computational Chemistry, Department of Chemistry, University of Tromsø, N-9037 Tromsø, Norway

[∥]Swedish e-Science Research Center (SeRC), Royal Institute of Technology, SE-100 44 Stockholm, Sweden

**ABSTRACT:** A density functional restricted−unrestricted approach, capable of evaluating hyperfine coupling constants with the inclusion of spin polarization effects in a spin-restricted Kohn−Sham method, has been extended to incorporate environmental effects. This is accomplished by means of a hybrid quantum mechanics/molecular mechanics formalism which allows for a granular representation of the polarization and electrostatic interactions with the classically described medium. By this technique, it is possible to trace the physical origin of hyperfine coupling constants in terms of spin polarization and spin density contributions and disentangle the dependence of these contributions on molecular geometry and solvent environment, something that increases the prospects for optimal design of spin labels for particular applications. A demonstration is given for the nitrogen isotropic hyperfine coupling constant in di-*tert*-butyl nitroxide solvated in water. The results indicate that the direct spin density contribution is about 5 times smaller than the spin polarization contribution to the nitrogen isotropic hyperfine coupling constant and that the latter contribution is solely responsible for the solvent shift of the constant. The developed approach is found capable of achieving satisfactory accuracy in prediction of the hyperfine coupling constants of solvated di-*tert*-butyl nitroxide and other similar nitroxides without the inclusion of solvent molecules in the quantum region provided polarizable force fields are used for the description of these molecules.

## 1. INTRODUCTION

Modeling of electron paramagnetic resonance (EPR) spin Hamiltonian parameters of nitroxide spin labels and related compounds has attracted considerable interest since the development of the first electronic structure methods for open shell molecules.[1−19] Over the years, numerous investigations of electronic **g** tensors[1,2,4,7−11,15,19] and hyperfine coupling tensors[1−3,5,6,8−18] have been carried out, and the mechanisms governing the behavior of EPR parameters of radicals in a vacuum and solutions have been thoroughly studied. Despite these achievements, the accurate prediction of electronic **g** tensors and especially hyperfine coupling constants of nitrogen in various nitroxides in protic solvents, like water or methanol, remains a challenge, as it requires a simultaneous account of solute vibrational degrees of freedom and solvent dynamics.[8,11−13,15,16,19] Recently, Barone and co-workers suggested a so-called integrated approach to overcome this kind of difficulty in the modeling of molecular properties[20] and successfully applied it to study several prototypical nitroxide radicals.[8,10,11,15,16] The essence of Barone et al.'s integrated approach is that the solute/solvent dynamics at a selected temperature are simulated using classical or Car−Parrinello (CP) molecular dynamics (MD) with the spin Hamiltonian parameters evaluated by means of density functional theory (DFT) over a set of snapshots extracted from the MD trajectory. Nowadays, approaches of this kind have been adopted by several groups interested in EPR spin Hamiltonian parameters of solvated radicals,[12,13,19,21,22] generating a steady increase of investigations.

The first part of the computations using the integrated approach, namely, the simulation of solute/solvent dynamics, is typically carried out by means of Car−Parrinello MD for short time scales, in the range of picoseconds,[8,11,19] or by means by classical MD for longer time scales, in the range of nanonseconds.[12−14] However, in the latter case, the applications are restricted to radicals for which classical force fields have been developed.[23,24] The second part of the computations in the integrated approach—the evaluation of electronic **g** tensors and hyperfine coupling tensors—has mostly been accomplished using unrestricted DFT combined with the polarizable continuum model (PCM) to account for the solvent environment.[8,11] Recently, hybrid density functional theory/molecular mechanics (DFT/MM) has emerged as an alternative to unrestricted DFT/PCM, and several applications of such methods for EPR spin Hamiltonian parameters of solvated nitroxides have now appeared.[12−14,19] Previously, one of us published an advanced QM/MM method based on the polarizable embedding scheme,[25] and in this paper, we extend this method to include calculations of hyperfine coupling constants of radicals.

**Received:** May 28, 2011
**Published:** August 17, 2011

Following our previous works devoted to the computation of hyperfine coupling constants of organic radicals and transition metal complexes,[26−28] we employ a density functional restricted−unrestricted (DFT-RU) approach and extend it into a hybrid quantum mechanics/molecular mechanics (QM/MM) setting. This work complements a recently implemented DFT/MM approach for the evaluation of electronic **g** tensors[19] and thus allows one to study the complete set of EPR spin Hamiltonian parameters of solvated nitroxide spin labels and other radicals with doublet ground states. Furthermore, this opens the possibility to substitute the conventional DFT/PCM method with the hybrid DFT/MM method in the integrated approach for studies of EPR spin Hamiltonian parameters in various environments, like proteins and cellular membranes, and thus to study such environmental effects on these parameters in greater detail and at a higher accuracy.

## 2. THE DENSITY FUNCTIONAL RESTRICTED−UNRESTRICTED APPROACH FOR SOLVENT ENVIRONMENTS

Spin-restricted DFT is designed to be spin-contamination-free, thus providing a starting formalism for EPR spin Hamiltonian parameters that from a conceptual point of view is more appropriate than the conventionally used unrestricted DFT, as it allows one to obtain a strict one-to-one mapping between the electron density and spin state of the molecule.[26−28] Despite this advantage, spin-restricted DFT methods have seldomly been used for the computation of hyperfine coupling constants, since they are incapable of accounting for spin polarization effects, which are of crucial importance for accurate prediction of these constants. Recently, we developed an extension of spin-restricted DFT—the so-called restricted−unrestricted approach, which follows the principles outlined in pioneering works by Fernández et al.[29,30] devoted to spin polarization effects in multiconfigurational self-consistent field calculations of molecular properties and allows one to account for spin polarization effects in calculations of linear and nonlinear molecular properties within a spin-restricted Kohn−Sham formalism.[26−28] This approach has been successfully applied to study electronic **g** tensors as well as hyperfine coupling constants of various organic radicals and transition metal complexes and has arguably provided comparable or better accuracy than the widely used unrestricted DFT methods. Our development of the DFT-RU approach has been focused on benchmarking its performance, and the modeling has thus been limited to a cluster approach in which the solvent molecules are treated explicitly along with the solute. In order to provide a more refined tool for investigation of the environmental effects on hyperfine coupling constants within the DFT-RU formalism, we implement in this work the hybrid DFT-RU/MM formalism based on the DFT/MM approach developed by Olsen et al.[25] In the remaining part of this section, we briefly review the basic principles behind the DFT-RU approach and describe the DFT-RU/MM extension, now implemented in a development version of the DALTON program.[31]

In DFT-RU, electronic spin-dependent properties, like hyperfine coupling constants, are typically computed as the sum of two terms:[26−28] one which accounts for the direct spin density contribution and the second which accounts for the spin polarization contribution to the property. More specifically, the expectation value in this approach for an arbitrary one-electron spin-dependent operator $\hat{A}$ can be written as

$$\langle \hat{A} \rangle = \langle \hat{A} \rangle_{\mathrm{den}} + \langle \hat{A} \rangle_{\mathrm{pol}} = \frac{\partial E[\rho(\mathbf{r},x),\tilde{\lambda},x]}{\partial x} + \tilde{\lambda}\frac{\partial^2 E[\rho(\mathbf{r},x),\tilde{\lambda},x]}{\partial x \partial \lambda} \quad (1)$$

where $\langle \hat{A} \rangle_{\mathrm{den}}$ and $\langle \hat{A} \rangle_{\mathrm{pol}}$ are the direct spin density and spin polarization contributions to the expectation value of operator $\hat{A}$, and $E[\rho(\mathbf{r},x),\tilde{\lambda},x]$ is the energy functional of the molecular system in the presence of a perturbation described by operator $\hat{A}$, which is dependent on the perturbed electron density $\rho(\mathbf{r},x)$, perturbation strength $x$, and set of Lagrangian multipliers $\tilde{\lambda} = (\bar{\kappa}_{pq}, \bar{t}_{pq})$ associated with singlet and triplet orbital rotations, which are collected into the set $\lambda = (\kappa_{pq}, t_{pq})$. The computation of $\langle \hat{A} \rangle_{\mathrm{den}}$ is a trivial task and is accomplished by contracting the unperturbed density $\rho(\mathbf{r},x = 0)$ with operator $\hat{A}$, while the evaluation of $\langle \hat{A} \rangle_{\mathrm{pol}}$ presents a more involved undertaking, as it requires the determination of Lagrangian multipliers $\tilde{\lambda}$ by solving

$$\frac{\partial^2 E[\rho(\mathbf{r},x),\tilde{\lambda},x]}{\partial \lambda^2}\tilde{\lambda} = -\frac{\partial E[\rho(\mathbf{r},x),\tilde{\lambda},x]}{\partial \lambda}\bigg|_{x=0} \quad (2)$$

Generally, in the approximate DFT-RU approach, the coupling between singlet and triplet orbital rotations can be neglected without a substantial loss of accuracy,[27] and thus the problem of finding Lagrangian multipliers $\tilde{\lambda}$ reduces to the task of finding Lagrangian multipliers associated with triplet orbital rotations by solving a set of linear equations

$$\frac{\partial^2 E[\rho(\mathbf{r},x),\tilde{\lambda},x]}{\partial t_{pq}^2}\bar{t}_{pq} = -\frac{\partial E[\rho(\mathbf{r},x),\tilde{\lambda},x]}{\partial t_{pq}}\bigg|_{x=0} = -\tau_{pq} \quad (3)$$

where the energy functional gradient $\tau_{pq}$ with respect to triplet orbital rotations $t_{pq}$ is nonvanishing in a spin-restricted Kohn−Sham formalism. The procedures for evaluation of triplet gradient elements, $\tau_{pq}$, and solving eq 2 or eq 3 are described in detail in our previous works devoted to the DFT-RU approach.[26−28] In the following, we outline modifications of the DFT-RU approach in the spirit of the recently developed DFT/MM method of Olsen et al.[25] required for enabling investigations of hyperfine coupling constants of solvated radicals.

The starting point to derive the DFT-RU/MM method is the Kohn−Sham Hamiltonian used by Olsen et al.[25] consisting of the conventional Kohn−Sham Hamiltonian describing the quantum region and a special coupling term between the quantum (QM) and classical (MM) regions

$$\hat{H} = \hat{H}_{\mathrm{QM}} + \hat{H}_{\mathrm{QM/MM}} \quad (4)$$

where $\hat{H}_{\mathrm{QM}}$ is defined in second quantization notation as

$$\hat{H}_{\mathrm{QM}} = \sum_{pq} f_{pq}\hat{E}_{pq} = \sum_{pq}(h_{pq} + j_{pq} + v_{pq}^{\mathrm{xc}})\hat{E}_{pq} \quad (5)$$

and where the coupling term $\hat{H}_{\mathrm{QM/MM}}$, which includes electrostatic and polarization interactions between QM and MM regions, is defined according to Olsen et al.[25] as

$$\hat{H}_{\mathrm{QM/MM}} = \sum_{pq}\sum_{s} M_{s,pq}^{(n)}\hat{E}_{pq} - \sum_{pq}\sum_{a}\boldsymbol{\mu}_a^{\mathrm{ind}}\mathbf{t}_{pq}^{a}\hat{E}_{pq} \quad (6)$$

In the above equations, we use notations frequently employed in density functional response theory for various matrix elements: $f_{pq}$

is the matrix element of the Kohn−Sham operator, which consists of the "core" Hamiltonian term $h_{pq}$, i.e., the sum of one-electron kinetic energy and nuclear attraction operators matrix elements, the Coulomb interaction term $j_{pq}$, and the exchange−correlation term $v^{xc}_{pq}$; $M^{(n)}_{s,pq}$ is an electrostatic interaction operator matrix element due to the $n$th order multipole at the site $s$ in the MM region (see eq 8 in ref 25 for the specific expression); $\boldsymbol{\mu}^{ind}_a$ is the induced dipole moment at the polarizable MM site $a$ created by the total (QM and MM) electric field at this site; $\mathbf{t}^a_{pq}$ is the matrix element of the electric field operator for site $a$ in the MM region; $\hat{E}_{pq} = p^\dagger_\alpha q_\alpha + p^\dagger_\beta q_\beta$ is the singlet excitation operator, which is in second quantization written as the combination of the spin-dependent creation operators for orbital $p$ and spin-dependent annihilation operators for orbital $q$. For a more detailed description of the enumerated quantities as well as the optimization procedures for the QM density and the MM induced dipole moments, we refer to the original work on the DFT/MM formalism.[25]

After describing the QM and QM/MM terms in the Kohn−Sham Hamiltonian of the unperturbed system, let us consider the situation in which the QM region also is affected by an electronic spin-dependent perturbation like the electron−nucleus Fermi contact interaction operator. In this case, the Hamiltonian becomes

$$\hat{H} = \hat{H}_{QM} + \hat{H}_{QM/MM} + x\hat{A} \tag{7}$$

where the spin-dependent perturbation operator in the general form can be written as

$$\hat{A} = \sum_m (-1)^m \sum_{pq} V^{-m}_{pq} T^m_{pq} \quad (m = -1, 0, 1) \tag{8}$$

with $V^{-m}_{pq}$ being the spherical component of the matrix element and $T^m_{pq}$ being the component of the triplet excitation operator associated with a corresponding element of electronic spin. Taking the form of the perturbation operator, the electron density of the perturbed system can, as shown in our previous works on the DFT-RU method,[26−28] be parametrized as

$$|\tilde{0}\rangle = \sum_{p>q} \exp[-\kappa_{pq}(\hat{E}_{pq} - \hat{E}_{qp})] \exp[-t_{pq}(\hat{T}_{pq} - \hat{T}_{pq})]|0\rangle \tag{9}$$

where $\kappa_{pq}$ and $t_{pq}$ are the parameters associated with singlet and triplet orbital rotations and $T_{pq}$ is the triplet excitation operator, i.e., $\hat{T}_{pq} = p^\dagger_\alpha q_\alpha - p^\dagger_\beta q_\beta$. Adopting this parametrization of the Kohn−Sham determinant in the case of the DFT-RU/MM approach, we can rewrite eq 3, which defines the spin polarization correction to the expectation value of the spin-dependent operator, as the set of linear equations

$$\mathbf{E}^{[2]}\bar{\mathbf{t}} = (\langle 0|[\hat{\mathbf{q}}, [\hat{\mathbf{q}}^\dagger, \hat{H}_{QM}] + \hat{H}^{(1)}_{QM}]|0\rangle + \langle 0|[\hat{\mathbf{q}}, [\hat{\mathbf{q}}^\dagger, \hat{H}_{QM/MM}] + \hat{H}^{(1)}_{QM/MM}]|0\rangle)\bar{\mathbf{t}} = -\tau \tag{10}$$

where $\hat{H}^{(1)}_{QM}$ and $\hat{H}^{(1)}_{QM/MM}$ are the QM and QM/MM contributions to the first-order perturbed Hamiltonian, the column $\bar{\mathbf{t}}$ is the collection of Lagrangian multipliers $\bar{t}_{pq}$ for triplet orbital rotations, $\bar{\mathbf{q}}^\dagger$ is the column vector of triplet excitation operators $\hat{T}_{pq}$, and $\tau$ is the energy functional $E[\rho(\mathbf{r}, 0), \tilde{\lambda}, 0]$ with respect to triplet orbital rotations with elements

$$\tau_{pq} = 2\langle 0|[\hat{T}_{pq}, \hat{H}_{QM}]|0\rangle + 2\langle 0|[\hat{T}_{pq}, \hat{H}_{QM/MM}]|0\rangle \tag{11}$$

In the latter two equations, we separated the orbital Hessian matrix $\mathbf{E}^{[2]}$ and triplet gradient $\tau_{pq}$ into QM and QM/MM contributions according to the partitioning of the Kohn−Sham Hamiltonian in eq 4. Procedures for determination of the triplet Lagrangian multipliers are described in detail in our previous works devoted to the DFT-RU approach.[26−28] The only two new elements introduced in eq 10 by extending the DFT-RU approach to a QM/MM setting are the QM and MM region coupling contributions from the Hamiltonian $\hat{H}_{QM/MM}$ to the $\mathbf{E}^{[2]}$ matrix and the $\tau$ column vector. The procedure for evaluation of the QM/MM contribution to the orbital Hessian in the DFT-RU/MM approach is exactly the same as the one used for linear triplet response functions in the DFT/MM formalism and has already been implemented in the DALTON program in connection with DFT/MM methods for the evaluation of nuclear spin−spin coupling constants[32] and triplet excitations energies.[33] Thus, only the $\hat{H}_{QM/MM}$ contribution to the triplet gradient (see eq 11) has been left to be implemented in this work in order to extend DFT-RU to the DFT-RU/MM setting. We accomplished this task by adapting subroutines used for evaluation of the orbital Hessian for the triplet response function to computation of the triplet gradient of the form given in eq 11.

After discussing the electronic spin-dependent properties within spin-restricted density functional theory using the restricted−unrestricted approach and presenting the details of extension of this formalism to the QM/MM setting, we describe in the remaining part of this work an application of the DFT-RU/MM method to study the isotropic hyperfine coupling constants of nitrogen in di-*tert*-butyl nitroxide (DTBNO) in aqueous solution.

## 3. COMPUTATIONAL DETAILS

For assessment of the DFT-RU/MM approach in prediction of the hyperfine coupling constants (HFCCs) of solvated radicals, we opted to study the isotropic HFCC of nitrogen in the prototypical nitroxide, namely di-*tert*-butyl nitroxide, in an aqueous environment. This choice is motivated by the availability of recent and detailed studies of nitrogen HFCCs in this system using unrestricted DFT/PCM and DFT/MM methods[8,13] as well as by results of our investigation of the electronic **g** tensor of this system using the DFT/MM formalism.[19] The latter work showed exceptional capabilities of the DFT/MM method to model a solvent environment using polarizable force fields. In this work, we determined the isotropic HFCC of nitrogen in DTBNO in aqueous solution at ambient temperature using the integrated approach proposed by Barone et al.[20] Thus, as the first step, a molecular dynamics simulation of DTBNO in water has been carried out using the hybrid Car−Parrinello/molecular mechanics method, and as the second step, the isotropic HFCC of nitrogen has been computed using the DFT-RU/MM method over a set of snapshots extracted from the MD trajectory generated in the first step. Details of both steps of computations for di-*tert*-butyl nitroxide in aqueous solution are given below.

**3.1. Hybrid Car−Parrinello/Molecular Mechanics Simulation of Di-*tert*-butyl Nitroxide in Aqueous Solution.** We have employed the hybrid Car−Parrinello/molecular mechanics (CP-MD/MM) approach[34,35] to generate the structures of di-*tert*-butyl nitroxide in aqueous solution at the ambient temperature. The details of this CP-MD/MM simulation have already been

given in our previous work[19] devoted to electronic **g** tensors of DTBNO, but for the sake of completeness, we repeat some key points here. In the CP-MD/MM simulation, only DTBNO has been treated at the density functional theory level using the BLYP exchange-correlation functional[36,37] and Troullier−Martins norm-conserving pseudopotentials[38] for the core electrons, and all 9679 waters have been moved to the MM region and described by the TIP3P force field.[39] The solute and solvent system, i.e., "DTBNO+9679 waters" has been included in an orthorhombic box with a size of approximately 68.4 Å × 65.8 Å × 65.4 Å, and the production run has been carried out for 21 ps in the canonical ensemble, where the temperature has been controlled using a Nosé−Hoover thermostat.[40,41] During this simulation, the following parameters were employed for the treatment of the QM region: the fictitious electronic mass was set to 600 amu; the integration time step was selected to be 5 au; the electronic wave function expansion cut off was set to 80 Ry. The initial structure for starting CP-MD/MM simulation was obtained from classical MD simulations as described in our previous work devoted to solvent effects on the electronic **g** tensor of DTBNO.[19]

**3.2. DFT-RU/MM Computations of Isotropic Hyperfine Coupling Constant of Nitrogen in Di-*tert*-butyl Nitroxide.** According to the philosophy of the integrated approach, we computed nitrogen ($^{14}$N isotope) isotropic hyperfine coupling constant, $a_N$, in DTBNO solvated in water by averaging $a_N$ evaluated using DFT-RU/MM over 86 snapshots taken from the CP-MD/MM trajectory. In these calculations and in analogy to our previous work devoted to the electronic **g** tensor of DTBNO,[19] we exploited two QM region models: one in which only DTBNO is included in the QM region and another in which DTBNO and two water molecules closest to the NO bond are included in the QM region. Similarly, the MM region has been designed to include all water molecules within the 20 Å radius of the DTBNO in order to ensure a converged description of the solvent environment, and five different types of force fields have been used to describe water molecules in the MM region. The selected force fields, denoted as MM-*X* (*X* = 0−4) in Table 1, follow the force fields ladder established in our previous work;[19] going from the MM-0 to the MM-4 force field provides a more accurate description of the water potential. Therefore, we carried out five different sets of calculations of the nitrogen HFCC for each QM region model by changing the force field description of the MM region. These calculations allow us to investigate the HFCC dependence on the accuracy of the MM description and to establish a requirement for the quality of the force field in the DFT-RU/MM calculations.

After giving the details of the MM region used in our DFT-RU/MM calculations, we turn to the QM region. In all calculations, we used the hybrid B3LYP[36,37,42,43] and PBE0[44,45] exchange−correlation functionals, which are known to be some of the most accurate functionals for evaluation of HFCCs in various organic radicals.[17,46−48] The second crucial choice is the selection of the basis set, as this basis set should be capable of describing accurately the electron density in the vicinity of the nucleus and at the same time be flexible enough in the outer valence region to account for spin polarization effects. One way to fulfill these requirements is to select a basis set augmented with tight *s*-type functions and several sets of polarization functions. We successfully employed this strategy in our previous studies of HFCCs of various organic radicals and paramagnetic transition metal complexes.[26−28] However, none of these studies included the nitroxides, and thus convergence of the nitrogen HFCCs with respect to Huz-X (X = IIII,IV) type basis sets[49,50] has not been investigated. In order to select a suitable basis set for our DFT-RU/MM calculations, we carried out an investigation of the basis set dependence of $a_N$ in the "DTBNO + 2 waters" system, in which the behavior of both the direct spin density contribution, $a_N^{den}$, and the spin polarization contribution, $a_N^{pol}$, with respect to basis set quality has been established. The results of this investigation are tabulated in Table 2 and indicate that $a_N$ converges going from the Huz-III basis set to the Huz-IIIsu3 basis set up to 0.04 G independently on the exchange−correlation functional used in calculations. Here, we point out that already using the Huz-III basis set an accurate description of the direct density contribution to $a_N$ is achieved and that only the spin polarization contribution is affected by improved description of the core region going from the Huz-III to the Huz-IIIsu3 basis set. Upon going from the Huz-III type basis sets to Huz-IV type basis sets, the description of the spin polarization contribution is further improved, indicating the importance of polarization functions for the accurate description of this contribution. The results clearly demonstrate that an accurate description of the spin polarization contribution is achieved only if the basis set used provides a balanced description of the inner core region and the outer valence region of atoms. Taking into account these findings and considering the computational cost, we performed all DFT-RU/MM calculations in this work using the Huz-IIIsu3 basis set. The selection of the exchange-correlation functional and basis set for description of the QM region in our DFT-RU/MM calculations is very similar to the one used in our studies of HFCCs in various organic radicals using the DFT-RU approach[26−28] and thus according to our experience should be adequate for nitrogen isotropic HFCCs in solvated DTBNO.

**Table 1. Hierarchy of the Force Fields Used to Describe the Water Molecules in DFT-RU/MM Calculations of Nitrogen Hyperfine Coupling Constant in Di-*tert*-butyl Nitroxide in Aqueous Solution**

| | electrostatics | | polarization | | |
|---|---|---|---|---|---|
| force field | multipoles | expansion points | polarization | expansion points | ref |
| MM-0 | charges | oxygen atom<br>hydrogen atoms | none | none | 39 |
| MM-1 | charges | oxygen atom<br>hydrogen atoms | isotropic | oxygen atom | 60 |
| MM-2 | charges | oxygen atom<br>hydrogen atoms | anisotropic | oxygen atom<br>hydrogen atoms | 19 |
| MM-3 | charges<br>dipoles<br>quadrupoles | oxygen atom<br>hydrogen atoms<br>OH midbonds[a] | anisotropic | oxygen atom<br>hydrogen atoms<br>OH midbonds | 19 |
| MM-4 | charges<br>dipoles<br>quadrupoles<br>octupoles | oxygen atom<br>hydrogen atoms<br>OH midbonds[a] | anisotropic | oxygen atom<br>hydrogen atoms<br>OH midbonds | 19 |

[a] Are not used as the expansion points for charges.

## 4. RESULTS AND DISCUSSION

We analyze in detail the performance of the DFT-RU/MM approach for the nitrogen isotropic hyperfine coupling constant in DTBNO in aqueous solution and compare the obtained

results with available experimental data[51−53] as well as results of recent studies by Pavone et al.[8] and by Houriez et al.[13] To start, we give a brief description of the nitrogen hyperfine coupling constants from the perspective of the DFT-RU approach.

**4.1. Isotropic Hyperfine Coupling Constant of Nitrogen in Nitroxides.** The EPR spin Hamiltonian parameters in nitroxides are governed to a large extent by the two molecular orbitals localized on the NO moiety of the nitroxide (see Figure 1), namely, a singly occupied orbital (SOMO) of $\pi$ type in which the unpaired electron resides and a doubly occupied orbital (HOMO) which accommodates a lone pair from oxygen. It has long been recognized that few states models,[54,55] which involve the SOMO and HOMO orbitals of nitroxide, explain the experimentally observed ordering of the electronic **g**-tensor components in these radicals or rationalize the solvent shift of the electronic the **g** tensor in various solvents in terms of a blue shift of the HOMO→SOMO excitation and electron density delocalization in the SOMO upon solvation.[51] Furthermore, the size of the nitrogen isotropic HFCC in nitroxides has been associated with the spin density distribution pattern in the SOMO orbital and its solvent behavior interpreted in terms of the selective stabilization of neutral or zwitterionic structure of the ONRR′ moiety by solvent molecules. Over the years, this picture of the physical mechanisms remained largely unchanged, and its validity has been verified many times by quantum chemical calculations.[4,5,7,8,19]

**Table 2. Basis Set Dependence of Nitrogen Isotropic HFCC in "DTBNO+ 2 waters" System in DFT-RU Calculations[a,b]**

| | B3LYP | | | PBE0 | | |
|---|---|---|---|---|---|---|
| basis set | $a_N^{den}$, G | $a_N^{pol}$, G | $a_N$, G | $a_N^{den}$, G | $a_N^{pol}$, G | $a_N$, G |
| Huz-III | 2.26 | 11.92 | 14.18 | 2.27 | 12.32 | 14.59 |
| Huz-IIIsu[c] | 2.23 | 11.84 | 14.07 | 2.24 | 12.42 | 14.66 |
| Huz-IIIsu1[d] | 2.26 | 12.03 | 14.30 | 2.27 | 12.64 | 14.91 |
| Huz-IIIsu2[e] | 2.26 | 12.12 | 14.39 | 2.29 | 12.71 | 15.00 |
| Huz-IIIsu3[f] | 2.28 | 12.14 | 14.43 | 2.29 | 12.75 | 15.04 |
| Huz-IV | 2.28 | 12.17 | 14.45 | 2.22 | 12.92 | 15.14 |
| Huz-IVsu4[g] | 2.27 | 12.33 | 14.60 | 2.28 | 12.94 | 15.22 |

[a] Nitrogen isotropic HFCC, $a_N$, has been computed as the average over 86 snapshots extracted from the CP-MD/MM trajectory. [b] All DFT-RU calculations have been performed using the hybrid B3LYP exchange−correlation functional. [c] All *s*-type functions have been uncontracted in the Huz-III basis set. [d] All *s*-type functions have been uncontracted in the Huz-III basis set, and one tight *s*-type basis function has been added according to procedure described in ref 61. [e] All *s*-type functions have been uncontracted in the Huz-III basis set, and two tight *s*-type basis functions have been added according to procedure described in ref 61. [f] All *s*-type functions have been uncontracted in the Huz-III basis set, and three tight *s*-type basis functions have been added according to the procedure described in ref 61. [g] All *s*-type functions have been uncontracted in the Huz-IV basis set, and four tight *s*-type basis functions have been added according to the procedure described in ref 61.

According to the above outlined interpretation, the nitrogen isotropic HFCC, $a_N$, in nitroxides is mostly dependent on the spin density distribution in the SOMO orbital localized on the NO bond. Thus, $a_N$ is inherently dependent on two geometrical parameters of the ONRR′ moiety (see Figure 1): the length of the NO bond and the improper dihedral angle $\theta$, which characterizes the NO bond tilt with respect to the NRR′ plane. From these two parameters, only the second one is important for the nitrogen isotropic HFCC, as the variation of the first parameter, the NO bond length, only weakly influences the size of $a_N$ in DTBNO and other nitroxides according to a recent study of Pavone et al.,[8] while changes in the second parameter, the improper angle $\theta$, strongly affect $a_N$ and increase more than twice with $\theta$ going from 0 to ±60° (see Figure 2) according to our DFT-RU calculations. Such a sharp dependence of nitrogen isotropic HFCC on the out-of-plane motion of the NO bond has already been observed in previous works,[8,12] and an accurate description of this effect has been found to be a key factor defining the overall reliability of computed nitrogen HFCCs. However, most of the previous studies have been carried out at the unrestricted DFT level, and thus a detailed analysis of the behavior of the direct spin density and spin polarization contributions to $a_N$ under the NO bond out of plane motion was impossible. In order to fill this gap, we carried out DFT-RU calculations of the nitrogen isotropic HFCC in DTBNO for different values of the improper dihedral angle, $\theta = -60$ to $+60$ . In Figure 2, we plotted both direct density, $a_N^{den}$, and spin

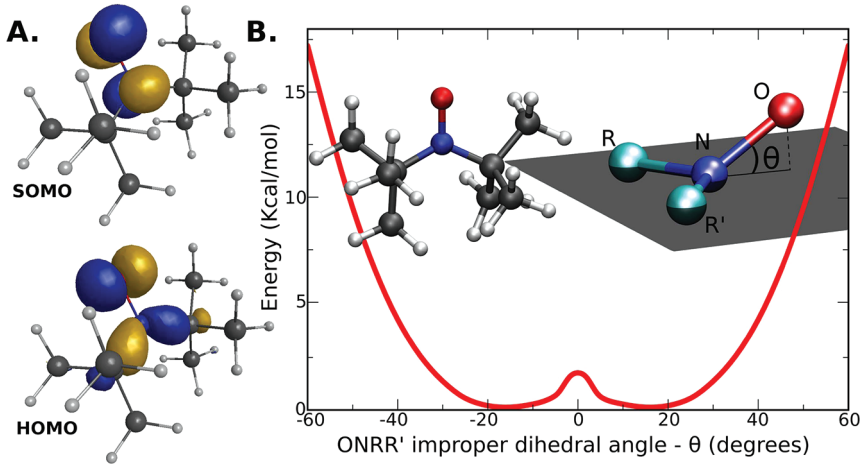


**Figure 1.** Key features of the electronic and geometrical structure of di-*tert*-butyl nitroxide. (A) Isosurface plots of $\pi$-type SOMO and *n*-type HOMO orbitals localized on the NO bond. (B) Potential energy surface for improper dihedral angle $\theta$ obtained by performing a relaxed potential energy surface scan with the spin-restricted open-shell MP2 method[56] using Ahlrich et al.'s TZVP basis set.[62] These calculations have been carried out using the GAMESS-US program.[63]

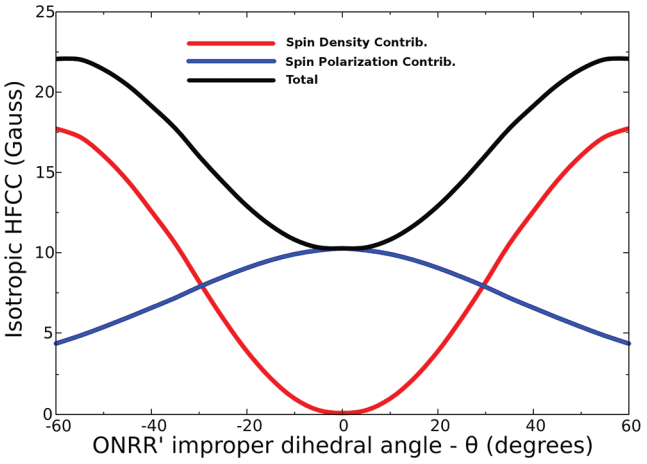


**Figure 2.** Dependence of nitrogen isotropic HFCC in di-*tert*-butyl nitroxide on the improper dihedral angle $\theta$ obtained using DFT-RU method at the B3LYP/Huz-IIIsu3 level.

polarization, $a_N^{pol}$, contributions to the $a_N$ dependence on improper dihedral angle $\theta$. As expected, Figure 2 shows the typical nitrogen isotropic HFCC dependence on the NO bond out of plane motion; i.e., the $a_N$ dependence on the improper dihedral angle $\theta$ has a parabolic shape with a minimum at the planar geometry of the ONRR′ moiety, and our DFT-RU results are consistent with previous findings obtained for various nitroxides at the unrestricted DFT level.[8,12] Here, we would like to point out that, from the two contributions constituting the nitrogen isotropic HFCC, only the direct spin density contribution $a_N^{den}$ exhibits a similar dependence on the improper dihedral angle $\theta$ to the isotropic HCCC itself (see Figure 2), while the spin polarization contribution $a_N^{pol}$ behaves completely differently and slowly decreases with the increase of the absolute value of the improper dihedral angle $\theta$ (see Figure 2). A closer inspection of Figure 2 reveals that the spin polarization contribution dominates $a_N$ for the small values of the improper dihedral angle $\theta$, as the $\pi$-type SOMO orbital localized on the NO bond in such a geometrical arrangement of the ONRR′ moiety does not provide efficient pathways for the generation of a sizable direct spin density contribution to $a_N$. However, for larger values of the improper dihedral angle $\theta$, $a_N^{den}$ sharply increases and becomes larger than the spin polarization contribution $a_N^{pol}$ for $\theta > 30$ (see Figure 2). Thus, the composition of the nitrogen isotropic HFCC in DTBNO as well as other nitroxides is directly controlled by the nonplanarity of the ONRR′ moiety, and for typical values of the improper dihedral angle $\theta = 10-20°$, the nitrogen isotropic HFCC is dominated by the spin polarization contribution, while the direct spin density contribution plays only a minor role amounting only up to 10−30% of $a_N$ values. The prominent role of spin polarization in nitrogen isotropic HFCC is an important finding, which gives a different interpretation of the shift of $a_N$ upon solvation as an adjustment to the change of spin density relaxation caused by solute interaction with solvent molecules. We will return to this topic and discuss it in the section devoted to the solvent shift of nitrogen isotropic HFCCs.

There are two different views on the shape of the potential energy surface (PES) associated with the NO bond out of plane motion. It is widely accepted that in most nitroxides the ONRR′ moiety is nonplanar and that the PES with respect to this degree of freedom is a symmetric or an asymmetric double well potential depending on the structure of the R and R′ groups in the specific nitroxide.[5,8,12,13] Typically, the barrier between the two wells is small and does not exceed a few kilocalories per mole, and at ambient temperature both wells are occupied with the NO bond continuously flipping between two minima. This conventional description of the PES associated with out of plane motion of the NO bond in DTBNO and 2,2,5,5-tetramethylpyrrolidine-N-oxyl has been recently challenged by Houriez and co-workers.[13] On the basis of B3LYP/6-311+G(d,p) calculations, they proposed that the PES associated with the improper dihedral angle has a harmonic potential shape with a single minimum at $\theta = 0$ and exhibits a flat energy profile around the minimum. These findings are though quite surprising and contradict the geometry optimization results of Pavone et al.,[8] Rinkevicius et al.[4,19] and Sinnecker et al.,[7] which all show that DTBNO has a nonplanar ONRR′ moiety at the equilibrium geometry. In order to settle this issue, we carried out a relaxed PES scan along the improper dihedral angle $\theta$ in DTBNO (see Figure 1) using the restricted open-shell MP2 method.[56] As one can see from Figure 1, our MP2 results clearly indicate that the PES associated with the motion of the NO bond in DTBNO has two wells and that the barrier between the wells is around 1.4 kcal/mol. On the basis of these findings, we will use a double well potential model for the PES associated with the NO bond out of plane motion in the interpretation of the nitrogen isotropic HFCC in DTBNO.

**4.2. Structure and Local Solvent Dynamics of Di-*tert*-butyl Nitroxide in Aqueous Solution.** According to the discussion in the previous section, the nitrogen isotropic HFCCs critically depend on the geometric structure of the ONRR′ moiety, and an understanding of changes of these geometrical parameters upon solvation is critical for interpretation of the solvent induced shifts of the HFCCs. In previous works,[8,13] both classical MD and Car−Parrinello MD have been employed to study the structure of DTBNO in aqueous solution. From these works, Car−Parrinello MD simulations by Pavone et al.[8] are the most rigorous ones, as they avoid empirical parametrization of the classical force field of DTBNO used in classical MD[13] and can thus model the internal molecular geometry of DTBNO and its solvent dependence more accurately compared to classical force-field-based approaches. However, the CP-MD method, being a pure density functional theory approach, neglects the dispersion interaction between the solute and solvent molecules as well as between the solvent molecules itself. In order to avoid this problem, we employed a hybrid CP-MD/MM method[34,35] for simulation of the DTBNO in aqueous solution, which supposedly yields better results in describing the solute−solvent supermolecular structures, as it includes all important solute/solvent interactions—short-range repulsion, long-range dispersion, and electrostatic interactions. In the following, we will analyze the intramolecular geometry of DTBNO in solution and its solvation shell structure obtained in our CP-MD/MM simulation and compared with previous CP-MD results by Pavone et al.[8] In Table 3, we list a few of the important internal geometrical parameters for DTBNO in aqueous solution obtained from our CP-MD/MM and previous CP-MD simulations. Interestingly, the internal geometry of DTBNO appears to be very similar in both CP-MD/MM and previous CP-MD simulations. However, the hybrid CP-MD/MM simulations predict a small increase in NO, NR, and NR′ bond lengths (when compared to CP-MD results), and this naturally should be attributed to the increased solute−solvent interaction strength within the QM/MM framework. A similar solvent-induced

**Table 3. Geometrical Structure of Di-*tert*-butyl Nitroxide in Aqueous Solution from Hybrid CP-MD/MM and CP-MD Simulations at Ambient Temperature**

| structural parameter[a] | CP-MD[b] | CP-MD/MM[c] | hydrogen bonds | CP-MD[b] | CP-MD/MM[c] |
|---|---|---|---|---|---|
| $R_{NO}$,[d] Å | 1.31 | 1.32 | number of H bonds | 1.2 | 1.3 |
| $\tilde{R}_{NR}$,[e] Å | 1.54 | 1.57 | $R_{NO\cdots O}$,[h] Å | 2.9 | 2.9 |
| ∠RNR′, deg | 127 | 130 | $R_{NO\cdots H}$,[i] Å | 1.9 | 1.9 |
| ∠$\tilde{O}$NR,[f] deg | 115 | 116 | ∠O···OH,[j] deg | 15 | 18 |
| $\lvert\theta\rvert$,[g] deg | 14.33 | 14.33 | | | |

[a] Structural parameter values are averaged over CP-MD or CP-MD/MM trajectory. [b] Results are taken from work by Pavone et al.[8] [c] This work. See Computational Details section. [d] $R_{NO}$ is the NO bond length in DTBNO. [e] $\tilde{R}_{NR}$ is the average of NR and NR′ bond lengths in DTBNO. [f] ∠$\tilde{O}$NR is the average of angles ONR and ONR′ in DTBNO. [g] $\lvert\theta\rvert$ is the absolute value of the improper dihedral angle, which describes NO bond motion out of the RNR′ plane (see Figure 1). [h] $R_{NO\cdots O}$ is the averaged distance between the oxygen atom of the NO group in DTBNO and the oxygen atom of the hydrogen bonded water molecule. [i] $R_{NO\cdots H}$ is the averaged hydrogen bond length between the NO group in DTBNO and the water molecule. [j] ∠O···OH is the characteristic hydrogen bonding angle between oxygen of NO group in DTBNO and OH bond in hydrogen bonded water molecule.

stretching of bond lengths due to intermolecular hydrogen bonding has been reported in the literature previously in the case of acetone and phenol blue.[57,58] It is interesting to note that the absolute value of the improper dihedral angle $\theta$ is the same in the case of CP-MD and CP-MD/MM simulations. The solute−solvent interactions as per the CP-MD and hybrid CP-MD/MM approaches are different with respect to dispersion and repulsion interaction energies; however, this brings only small changes in the internal molecular geometry around the ONRR′ moiety. The NO bond length differs by 0.01 Å, while the average of NR and NR′ bond lengths differs by 0.03 Å. Thus, overall, the geometrical structure of DTBNO obtained in our CP-MD/MM simulations is very similar to the one featured in CP-MD simulations of Pavone et al.[8]

Apart from the above-described structural parameters of DTBNO in aqueous solution, the local solvent structure around DTBNO also plays an important role in defining the solvent shift of nitrogen isotropic HFCC in this radical. Taking this into account, we focus on the structure of the first solvation shell since the solvent molecules in this shell are known to be most influential on the EPR spin Hamiltonian parameters of nitroxides, as they are in direct contact with the nitroxides through intermolecular hydrogen bonding and charge transfer. In the previous work by Pavone et al.,[8] the first solvation shell was characterized in terms of the number of solvent molecules in hydrogen bonding with the DTBNO and the geometry of this intermolecular hydrogen bonding. In order to facilitate a direct comparison with their results, we have adopted the same geometrical parameters to define the hydrogen bonding.[8] A solvent molecule is said to be hydrogen bonding with a solute molecule when the following three conditions are fulfilled: (a) $R_{NO\cdots O} \leq 3.5$ Å, (b) $R_{NO\ldots H} \leq 2.6$ Å, and (c) ∠O···OH ≤ 30°. Figure 3 shows the populations of solute−solvent supermolecular structures in our CP-MD/MM simulation, where the number of intermolecular hydrogen bonding varies between 0 and 3. Interestingly, the average bond lengths between DTBNO and hydrogen-bonded water molecules ($R_{NO\cdots O}$ and $R_{NO\cdots H}$ in Table 3) appear to be the same for both, CP-MD and CP-MD/MM, approaches. Even the averaged characteristic angle, ∠O···OH, is the same in both cases, suggesting that the average solute/solvent local structure is the same. However, as it is seen from Figure 3, the dynamical pictures of solute−solvent structure captured by these two approaches are quite different. The CP-MD approach could not find any solute−solvent structure with three hydrogen bonds between the solute and solvent molecules, while the hybrid CP-MD/MM approach predicts the population of such structures to be around 7%. Moreover, the solute−solvent structures with zero hydrogen bonding are more populated in the case of hybrid CP-MD/MM simulations. Both approaches predict an almost equal population for the solute−solvent structures with two hydrogen bonds. The average number of hydrogen bonds in the solute−solvent structures is 1.2 in the case of the CP-MD approach, while it is 1.3 in the case of the hybrid CP-MD/MM approach, and so the latter approach predicts a slightly larger coordination number for hydrogen-bonded solvent molecules. Overall, the results suggest that the average (intermolecular) geometry of solute−solvent structure is the same as obtained from both approaches, while the dynamic description of this is very different in both cases. Here, we notice that a similar situation has been encountered in modeling of the copper dication solvation in water,[59] where the CP-MD/MM approach predicted a six coordinated structure while the CP-MD-approach-based simulations predicted a five coordinated structure, and where the structure from the latter approach has been discussed to be an artifact due to the neglect of dispersion interactions. In the forthcoming section, we will discuss the nitrogen isotropic HFCC obtained by averaging over a set of snapshots from the above-described CP-MD/MM simulations and investigate the influence of the local solvent

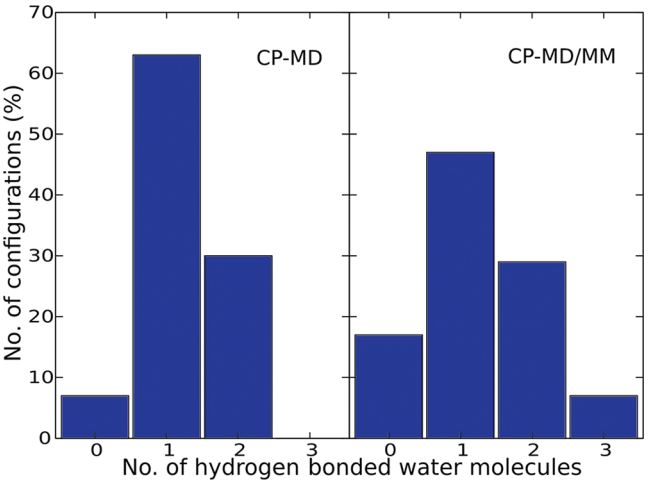


**Figure 3.** Hydrogen bonding patterns of di-*tert*-butyl nitroxide in aqueous solution at ambient temperature obtained from CP-MD (Pavone et al.[8]) and CP-MD/MM (this work) simulations.

environment around the solute on this EPR spin Hamiltonian parameter.

**4.3. Isotropic Hyperfine Coupling Constant of Nitrogen in Di-*tert*-butyl Nitroxide in Aqueous Solution.** After describing the isotropic HFCC of nitrogen in DTBNO from the perspective of the DFT-RU approach and analyzing the geometrical structure of DTBNO in aqueous solution, let us turn to the main topic of this work, namely, the capability of the DFT-RU/MM approach to predict the nitrogen isotropic HFCC in DTBNO solvated in water. First, we will discuss the dependence of the nitrogen isotropic HFCC on the description of the MM region and, later on, compare our results with experimental data[51−53] as well as findings from previous works[8,13] which exploited the integrated approach.[20]

In Table 4, we give the isotropic HFCC of nitrogen in DTBNO in water computed by DFT-RU/MM. First, we consider the simplest possible model of the QM region, which contains only the DTBNO radical and with all water molecules within a 20 Å radius moved to the MM region. As expected, according to our analysis of the nitrogen isotropic HFCC in DTBNO, the direct spin density contribution constitutes only 14.5−17.2% of the total $a_N$ value, averaged over 86 snapshots, depending on the MM region treatment and on the exchange-correlation functional (see Table 4), and the remaining contribution to the $a_N$ value originates from the spin polarization contribution. We point out that such a $a_N$ composition, with some minor variations in terms of direct spin density and spin polarization contributions, is observed from most of the snapshots used in our DFT-RU/MM calculations, and only for a few snapshots in which the improper dihedral angle $\theta$ is large does the direct spin density contribution to $a_N$ turn out to be larger than the spin polarization contribution.

After establishing the composition of the nitrogen isotropic HFCC in DTBNO, we turn to its solvent shift. As one can see from Table 4, the DFT-RU/MM approach predicts the solvent shift of $a_N$, depending on the force field used in the water MM region, to be 1.98−2.65 G at the B3LYP level and 2.19−2.94 G at the PBE0 level, respectively. For the crudest description by the MM-0 force field, which contains only point charges, the calculations at the B3LYP level predict the solvent shift to be 1.98 G or around 15% of the $a_N$ value in a vacuum. A slightly larger solvent shift, equal to 2.19 G, is obtained at the PBE0 level. Here, we would like to point out that the vibrational contribution from internal DTBNO dynamics to $a_N$ in our DFT-RU calculations is estimated to be 0.21 at the B3LYP level and, in agreement with the results of Pavone et al.,[8] is much smaller than the solvent shift. Exchanging MM-0 with the more elaborate MM-1 force field, which in addition to point charges also contains the isotropic water polarizability (see Table 1), turns out to have little effect on nitrogen isotropic HFCC. This is due to the fact that the MM-0 force field point charge values are constructed to mimic the solvent environment and account implicitly for polarization by artificially increasing the values of the point charges used to describe the water molecules. Further improvement of the force field from MM-1 to MM-2, which introduces distributed anisotropic polarizability tensors in the description of water molecules in the MM region, leads to a significant increase in the solvent solvent shift of $a_N$ by almost 20−23% depending on the exchange−correlation functional compared to the one obtained in the calculations with the MM-0 or MM-1 force fields. Finally, the last two force fields, MM-3 and MM-4, which go beyond the point charge approximation and also provide more refined water polarizability by using more expansion points, give almost identical HFCC values (see Table 4) and predict the $a_N$ solvent shift at the B3LYP level to be 2.62 or 2.65 G, which is around 8% larger than the solvent shift predicted using the MM-2 force field. Similar results are also obtained with the PBE0 functional, which gives a solvent shift for MM-3 and MM-4 force fields of 2.91 and 2.94 G, respectively. Taking these results into account, we conclude that the solvent shift of the nitrogen isotropic HFCCs in DTBNO is highly dependent on the quality of the force field used for the description of the MM region; independently of the exchange−correlation functional used, its value increases going from the MM-0 to the MM-4 force field in the order MM-0 ≈ MM-1 < MM-2 < MM-3 ≈ MM-4. Thus, the MM-3 force field provides a converged description of the water potential in the DFT-RU/MM calculations in which the QM region is limited to the solute itself, and force fields designed

**Table 4. Isotropic Hyperfine Coupling Constant of Nitrogen of the Di-*tert*-butyl Nitroxide in Water Computed with DFT/MM Methods Employing Two QM Regions: One Which Includes Only Di-*tert*-butyl Nitroxide and Another Which Includes Di-*tert*-butyl Nitroxide with Two Water Molecules Hydrogen Bonded to the NO Bond[a,b]**

| | DTBNO | | | DTBNO+2$H_2O$ | | |
|---|---|---|---|---|---|---|
| method | $a_N^{den}$, G | $a_N^{pol}$, G | $a_N$, G | $a_N^{den}$, G | $a_N^{pol}$, G | $a_N$, G |
| B3LYP | 2.26 | 10.86 | 13.12 | 2.28 | 12.14 | 14.43 |
| B3LYP/MM-0 | 2.34 | 12.75 | 15.10 | 2.32 | 12.90 | 15.23 |
| B3LYP/MM-1 | 2.33 | 12.82 | 15.15 | 2.32 | 12.90 | 15.23 |
| B3LYP/MM-2 | 2.34 | 13.21 | 15.55 | 2.32 | 13.08 | 15.40 |
| B3LYP/MM-3 | 2.36 | 13.38 | 15.74 | 2.33 | 13.14 | 15.47 |
| B3LYP/MM-4 | 2.36 | 13.41 | 15.77 | 2.32 | 13.15 | 15.48 |
| PBE0 | 2.24 | 11.32 | 13.56 | 2.29 | 12.75 | 15.04 |
| PBE0/MM-0 | 2.36 | 13.39 | 15.75 | 2.34 | 13.59 | 15.93 |
| PBE0/MM-1 | 2.35 | 13.46 | 15.81 | 2.34 | 13.59 | 15.93 |
| PBE0/MM-2 | 2.36 | 13.91 | 16.27 | 2.35 | 13.77 | 16.12 |
| PBE0/MM-3 | 2.39 | 14.08 | 16.47 | 2.35 | 13.84 | 16.19 |
| PBE0/MM-4 | 2.39 | 14.11 | 16.50 | 2.35 | 13.86 | 16.21 |
| PBE0[c] | | | 13.1 | | | |
| PBE0/PCM[c] | | | 12.6 | | | 14.7 |
| PBE0[d] | | | 14.2 | | | |
| PBE0/ESPF[d] | | | 16.7 | | | |
| exptl.[e] | | | 16.75 ± 0.04 | | | 16.75 ± 0.04 |
| exptl.[f] | | | 17.18 ± 0.01 | | | 17.18 ± 0.01 |
| exptl.[g] | | | 17.16 ± 0.01 | | | 17.16 ± 0.01 |

[a] Nitrogen isotropic HFCC, $a_N$, has been computed as the average over 86 snapshots extracted from the CP-MD/MM trajectory. [b] All DFT-RU calculations have been performed using the hybrid B3LYP exchange−correlation functional and Huz-IIIsu3 basis set. [c] Unrestricted DFT results obtained for a vacuum and DFT/PCM results for water solution by Pavone et al.[8] Calculations were carried out using the EPR-II basis set, and results are averaged over snapshots extracted from the CP-MD trajectory. [d] Unrestricted DFT results obtained for a vacuum and DFT/ESPF results for water solution by Houriez et al.[13] Calculations were carried out using 6-31G+(d,p) basis set, and results are averaged over snapshots extracted from the classical MD trajectory. [e] Experimental data taken from work by Kawamura et al.[51] EPR spectra measurements have been carried out at ambient temperature. [f] Experimental data taken from work by Knauer and Napie.[53] EPR spectra measurements have been carried out at ambient temperature. [g] Experimental data taken from work by Griffith et al.[52] EPR spectra measurements have been carried out at ambient temperature.

using the same procedure can be recommended for general computations of hyperfine coupling constants in more complex environments.

After discussing the quality of the MM description in the case of the simplest QM model, which contains only one DTBNO molecule, we attend to the results obtained with a more complex QM region model, which includes the DTBNO radical and the two closest water molecules to the NO bond of DTBNO. This model of the QM region is frequently employed in DFT/PCM studies of various properties of nitroxides,[5] as it explicitly accounts for the hydrogen bonding between the nitroxide and solvent molecules and in turn allows one to study nitroxides in protic solvents within the DFT/PCM method. Thus, by comparing the DFT-RU results obtained using the two QM region models, we estimate that the hydrogen-bonding-induced solvent shift of $a_N$ in DTBNO is equal to 1.31 G at the B3LYP level and to 1.48 G at the PBE0 level, respectively. The remaining part of the solvent shift originates from the water molecules in the bulk, and according to our DFT-RU/MM results (see Table 4), this is, depending on the force field used, between 0.8 and 1.05 G for the B3LYP functional and between 0.89 and 1.17 G for the PBE0 functional. A closer inspection of the DFT-RU/MM results reveals that the solvent shift associated with water molecules in the MM region shows a similar behavior with respect to force field quality as in the above-discussed case and increases in the following order independently of the exchange−correlation functional used in calculations: MM-0 ≈ MM-1 < MM-2 < MM-3 ≈ MM-4. However, differences between results obtained with different force fields are less pronounced, since the water molecules which are most sensitive to the quality of the force field in this case are included in the QM region.

The QM region models, namely the one which includes only DTBNO and the other which includes "DTBNO+2 waters", behave rather similarly in DFT-RU/MM calculations, and differences between two models for the HFFCs do not exceed 0.29 G for both exchange-correlation functionals used in this work. For the lower quality force fields, MM-0 and MM-1, the second QM region model, which includes water molecules explicitly, gives rise to slightly larger $a_N$ values compared to the first QM region model, while the opposite holds for the other force fields used in this work. Here, we would like to point out that the differences between the two QM region models from the perspective of the overall accuracy of the nitrogen isotropic HFCC, obtained using the DFT-RU/MM approach, are rather small, and usage of the simpler QM region model introduces an error similar in size to the one obtained truncating the basis set from Huz-IVsu4 to Huz-IIIsu3 (see Table 2). Comparing the DFT-RU/MM results obtained for both QM region models (see Table 4), it is evident that the changes in the description of the waters hydrogen-bonded to DTBNO from quantum to classical affects only the changes of the spin polarization contribution to $a_N$, while the direct spin density contribution remains almost unchanged. It becomes clear that the question of which combination of the QM region model and force field is sufficiently accurate for routine calculations of nitrogen isotropic HFCCs in nitroxides and spin labels is nontrivial. From the conceptual point of view, the QM region model, which includes DTBNO and two hydrogen-bonded water molecules, and a force field parametrized in terms of distributed multipoles and anisotropic polarizability tensors, is the most suitable combination for DFT-RU/MM calculations. As we can see from Table 4, a converged description of the nitrogen isotropic HFCC in DTBNO for this QM region model is obtained already for the MM-3 force field. However, explicit inclusion of solvent molecules into the QM region is highly undesirable, as it significantly increases the computational cost and limits the applicability of the DFT-RU/MM method to complex environments, like cellular membranes or ion channels. Therefore, for practical applications of the DFT-RU/MM method, it would be advantageous to limit the QM region to the solute itself. A closer inspection of Table 4 reveals that combining the simpler QM region model, which includes only DTBNO, with the MM-2 force field gives $a_N$ values close to the converged ones computed using the more complex QM region model and MM-3 force field. On the basis of these findings, we can recommend limiting the QM region in practical DFT-RU/MM calculations to the nitroxide of interest and treating the environment with a force field of similar quality to that of the MM-2 force field for water. This recommendation relies on error cancellation between the description of the bulk part of the solvent environment and the hydrogen-bonded solvent molecules, and its validity must be tested further and especially for nonaqueous solutions.

After settling the issues with suitable QM region models and force fields for DFT-RU/MM calculations, let us turn our attention to the solvent-induced shift of this quantity. For both QM region models, our DFT-RU/MM calculations, independently of the force field used, show that the direct spin density contribution to $a_N$ is almost not at all affected by the solvation of DTBNO and that the solvent shift of the isotropic HFCC arises solely from the spin polarization contribution. This statement holds for most of the snapshots extracted from the CP-MD/MM trajectory, but for some snapshots in which the improper dihedral angle $\theta$ (see Figure 1) is large, the direct spin density contribution to $a_N$ can also exhibit a solvent shift. However, instantaneous configurations of DTBNO with large improper dihedral angles $\theta$ are rarely encountered in CP-MD/MM simulations at ambient temperature due to the steep PES for this degree of freedom (see Figure 1), and therefore they will have little impact on the overall behavior and size of the solvent shift of $a_N$.

After establishing the origin of the solvent shift of the nitrogen isotropic HFCC in DTBNO solvated in water, let us turn to the dependence of this shift on the solvent environment. From results presented in Table 4, we can estimate that the solvent shift of $a_N$ is around 2.35 G at the B3LYP level (QM region model: "DTBNO+2 waters" and MM-3 force field), where around 56% of the solvent shift originates from direct hydrogen bonding and the remaining part from bulk solvent. At the PBE0 level, the solvent shift is slightly larger and is around 2.63 G, but the relative size of hydrogen bonding and bulk solvent contributions remains similar to the B3LYP case. Unfortunately, a more detailed explanation of the spin polarization contribution to $a_N$ upon solvation is not easily achieved, as it turns out that many triplet orbital rotations contribute to the electron density relaxation. Finally, concluding the discussion of solvent shift of the nitrogen isotropic HFCC in DTBNO, we point out that our calculation results conform with the conventional explanation of this solvent shift as a consequence of the preferential stabilization of the zwitterionic form of the ONRR′ moiety. However, we would like to emphasize that the origin of the larger nitrogen isotropic HFCCs in the zwitterionic form is due to a more effective spin polarization and not because of an increase in the direct spin density contribution as has been suggested previously.

To complete our discussion of nitrogen isotropic HFCCs in DTBNO solvated in water, we compare the results obtained using our DFT-RU/MM approach with experimental data and

results from previous studies with the integrated approach. As we can see from Table 4, independently of the QM region model and force field used, the DFT-RU/MM approach underestimates the experimentally measured $a_N$ by 1.4−2.1 G at the B3LYP level and by 0.6−1.4 G at the PBE0 level. Thus, the PBE0 functional predicts nitrogen HFCCs in radicals with better accuracy than the commonly used B3LYP functional, as was already noted in previous works devoted to HFCCs.[17,48] Taking into account the strong dependence of the nitrogen isotropic HFCCs on the exchange−correlation functional and basis set used in specific DFT calculations, our DFT-RU/MM results compare quite well with data from the unrestricted DFT/PCM calculations of Pavone et al.[8] and unrestricted DFT/MM calculations of Houriez et al.[13] On the basis of this set of results, we can confirm that the DFT-RU/MM approach provides more accurate results than conventional unrestricted DFT-based approaches and that it thus can be recommended for studies of nitroxides in various complex environments.

## 5. CONCLUSIONS

In the present work, we have taken a critical step toward realistic modeling and design of molecular spin probes in solution or confined environments. Our work combines up-to-date electronic structure theory for open shell systems with new developments of multiscale modeling techniques for solvent interactions. The former encompasses a density functional theory that "solves" the spin problem in that the reference state can be maintained spin-uncontaminated, thus allowing one to obtain a strict one-to-one mapping between electron density and spin state of the molecule, yet proper spin polarization is introduced in the calculation of the property. This, the so-called restricted−unrestricted DFT approach earlier introduced by the authors, has shown good performance in prediction of spin Hamiltonian parameters, including the hyperfine coupling constant addressed in the present work. We then used a QM/MM response theory with a full account of intermolecular interaction for the quantum mechanical property of the solute.

A demonstration is given for the nitrogen isotropic hyperfine coupling constant in di-*tert*-butyl nitroxide solvated in water for which we in detail investigated the representation of the QM and MM regions required for an accurate prediction of this constant, thus the need for additional hydrogen-bonded molecules treated quantum mechanically and the degree of granularity in the charge and polarizability distributions of the MM water molecules. It is found that an accurate MM force field reduces the need to include explicit water molecules in the QM region, something that significantly decreases computation cost and widens the applicability to more complex environments. The DFT-RU/MM technique allowed us to pinpoint the origin of the solvent shift in great detail: Part of the solvent dependence originates in that the nitrogen isotropic HFCC critically depends on the geometrical structure of the ONRR′ moiety and that these geometrical parameters change rather significantly upon solvation. Moreover, only the direct spin density contribution to the nitrogen isotropic HFCC exhibits a similar dependence on NO bond out of plane motion to that of the isotropic HCCC itself, while the spin polarization contribution behaves very differently and slowly decreases with the increase of the absolute value of the improper dihedral angle between the NO bond and NRR′ moiety. The prominent role of spin polarization is an important finding, which gives the interpretation of the shift of nitrogen isotropic HFCC upon solvation as an adjustment to the change of spin density relaxation, i.e., spin polarization change caused by solute interaction with solvent molecules.

We find that the RU-DFT/MM methods allow one to calculate nitroxoide HFFCs with good accuracy at the same time as it provides interpretation to the dependence on electron and geometrical structure and solvent environment. In particular, the ability of the method to separate the spin polarization from the direct spin density contributions allows one to disentangle the structure−property relations for these constants. This in turn is an important aspect when turning to more complex, confined environments, like protein cavities or membrane channels, where application-specific design of the nitroxide spin labels with optimal performance is desirable.

## AUTHOR INFORMATION

**Corresponding Author**
*E-mail: rinkevic@theochem.kth.se.

## ACKNOWLEDGMENT

This work has been partially funded by the EU Commission (contract INFSO-RI-261523) under the ScalaLife collaboration and has been supported by a grant from the Swedish Infrastructure Committee (SNIC) for the project "Multiphysics Modeling of Molecular Materials", SNIC 022/09-25. J.K. thanks The Danish Councils for Independent Research and the Lundbeck Foundation for financial support.

## REFERENCES

(1) Owenius, R.; Engström, M.; Lindgren, M.; Huber, M. *J. Phys. Chem. A* **2001**, *105*, 10967–10977.
(2) Engström, M.; Vaara, J.; Schimmelpfennig, B.; Ågren, H. *J. Phys. Chem. B* **2002**, *106*, 12354–12360.
(3) D'Amore, M.; Improta, R.; Barone, V. *J. Phys. Chem. A* **2003**, *107*, 6264–6269.
(4) Rinkevicius, Z.; Telyatnyk, L.; Vahtras, O.; Ruud, K. *J. Chem. Phys.* **2004**, *121*, 5051–5060.
(5) Improta, R.; Barone, V. *Chem. Rev.* **2004**, *104*, 1231–1254.
(6) Neugebauer, J.; Louwerse, M. J.; Belanzoni, P.; Wesolowski, T. A.; Baerends, E. J. *J. Chem. Phys.* **2005**, *123*, 114101.
(7) Sinnecker, S.; Rajendran, A.; Klamt, A.; Diedenhofen, M.; Neese, F. *J. Phys. Chem. A* **2006**, *110*, 2235–2245.
(8) Pavone, M.; Cimino, P.; De Angelis, F.; Barone, V. *J. Am. Chem. Soc.* **2006**, *128*, 4338–4347.
(9) Barone, V.; Brustolon, M.; Cimino, P.; Polimeno, A.; Zerbetto, M.; Zoleo, A. *J. Am. Chem. Soc.* **2006**, *128*, 15865–15873.
(10) Carlotto, S.; Cimino, P.; Zerbetto, M.; Franco, L.; Corvaja, C.; Crisma, M.; Formaggio, F.; Toniolo, C.; Polimeno, A.; Barone, V. *J. Am. Chem. Soc.* **2007**, *129*, 11248–11258.
(11) Pavone, M.; Cimino, P.; Crescenzi, O.; Sillanpää, A.; Barone, V. *J. Phys. Chem. B* **2007**, *111*, 8928–8939.
(12) Houriez, C.; Ferré, N.; Masella, M.; Siri, D. *J. Chem. Phys.* **2008**, *128*, 244504.
(13) Houriez, C.; Ferré, N.; Siri, D.; Masella, M. *J. Phys. Chem. B* **2009**, *113*, 15047–15056.
(14) Houriez, C.; Ferré, N.; Masella, M.; Siri, D. *THEOCHEM* **2009**, *898*, 49–55.
(15) Pavone, M.; Biczysko, M.; Rega, N.; Barone, V. *J. Phys. Chem. B* **2010**, *114*, 11509–11514.
(16) Barone, V.; Cimino, P.; Pedone, A. *Magn. Reson. Chem.* **2010**, *48*, S11–S22.
(17) Hermosilla, L.; García de la Vega, J. M.; Sieiro, C.; Calle, P. *J. Chem. Theory Comput.* **2011**, *7*, 169–179.

(18) Ikryannikova, L. N.; Ustynyuk, L. Y.; Tikhonov, A. N. *Magn. Reson. Chem.* **2010**, *48*, 337–349.
(19) Rinkevicius, Z.; Murugan, N. A.; Kongsted, J.; Aidas, K.; Steindal, A. H.; Ågren, H. *J. Phys. Chem. B* **2011**, *115*, 4350–4358.
(20) Crescenzi, O.; Pavone, M.; De Angelis, F.; Barone, V. *J. Phys. Chem. B* **2005**, *109*, 445–453.
(21) Asher, J. R.; Kaupp, M. *Theor. Chem. Acc.* **2008**, *119*, 477–487.
(22) Pauwels, E.; Declerck, R.; Verstraelen, T.; De Sterck, B.; Kay, C. W. M.; Van Speybroeck, V.; Waroquier, M. *J. Phys. Chem. B* **2010**, *114*, 16655–16665.
(23) Sezer, D.; Freed, J. H.; Roux, B. *J. Phys. Chem. B* **2008**, *112*, 5755–5767.
(24) Stendardo, E.; Pedone, A.; Cimino, P.; Menziani, M. C.; Crescenzi, O.; Barone, V. *Phys. Chem. Chem. Phys.* **2010**, *12*, 11697–11709.
(25) Olsen, J. M.; Aidas, K.; Kongsted, J. *J. Chem. Theory Comput.* **2010**, *6*, 3721–3734.
(26) Rinkevicius, Z.; Telyatnyk, L.; Vahtras, O.; Ågren, H. *J. Chem. Phys.* **2004**, *121*, 7614–7623.
(27) Oprea, C. I.; Telyatnyk, L.; Rinkevicius, Z.; Vahtras, O.; Ågren, H. *J. Chem. Phys.* **2006**, *124*, 174103.
(28) Rinkevicius, Z.; de Almeida, K. J.; Vahtras, O. *J. Chem. Phys.* **2008**, *129*, 064109.
(29) Fernandéz, B.; Jørgensen, P.; Byberg, J.; Olsen, J.; Helgaker, T.; Jensen, H. J. A. *J. Chem. Phys.* **1992**, *97*, 3412–3419.
(30) Fernández, B.; Christiansen, O.; Bludsky, O.; Jørgensen, P.; Mikkelsen, K. V. *J. Chem. Phys.* **1996**, *104*, 629–635.
(31) DALTON program. www.daltonprogram.org (accessed Aug 2011).
(32) Møgelhøj, A.; Aidas, K.; Mikkelsen, K. V.; Sauer, S. P. A.; Kongsted, J. *J. Chem. Phys.* **2009**, *130*, 134508.
(33) Aidas, K.; Mikkelsen, K. V.; Mennucci, B.; Kongsted, J. *Int. J. Quantum Chem.* **2011**, *111*, 1511–1520.
(34) Laio, A.; VandeVondele, J.; Rothlisberger, U. *J. Phys. Chem. B* **2002**, *106*, 7300–7307.
(35) Laio, A.; VandeVondele, J.; Rothlisberger, U. *J. Chem. Phys.* **2002**, *116*, 6941–6947.
(36) Becke, A. D. *Phys. Rev. A* **1988**, *38*, 3098–3100.
(37) Lee, C.; Yang, W.; Parr, R. G. *Phys. Rev. B* **1988**, *37*, 785–789.
(38) Troullier, N.; Martins, J. L. *Phys. Rev. B* **1991**, *43*, 1993–2006.
(39) Jorgensen, W. L.; Chandrasekhar, J.; Madura, J. D.; Impey, R. W.; Klein, M. L. *J. Chem. Phys.* **1983**, *79*, 926–935.
(40) Nosé, S. *J. Chem. Phys.* **1984**, *81*, 511–519.
(41) Hoover, W. G. *Phys. Rev. A* **1985**, *31*, 1695–1697.
(42) Becke, A. D. *J. Chem. Phys.* **1993**, *98*, 5648–5652.
(43) Vosko, S. H.; Wilk, L.; Nusair, M. *Can. J. Phys.* **1980**, *58*, 1200–1211.
(44) Perdew, J. P.; Ernzerhof, M.; Burke, K. *J. Chem. Phys.* **1996**, *105*, 9982–9985.
(45) Perdew, J. P.; Burke, K.; Ernzerhof, M. *Phys. Rev. Lett.* **1996**, *77*, 3865–3868.
(46) Hermosilla, L.; Calle, P.; García de la Vega, J. M.; Sieiro, C. *J. Phys. Chem. A* **2005**, *109*, 1114–1124.
(47) Barone, V.; Cimino, P.; Stendardo, E. *J. Chem. Theory Comput.* **2008**, *4*, 751–764.
(48) Barone, V.; Cimino, P. *Chem. Phys. Lett.* **2008**, *454*, 139–143.
(49) van Wüllen, C. *Die Berechnung magnetischer Eigenschaften unter Berücksichtigung der Eletronkorrelation: Die Multikonfigurations-Verallgemeinerung der IGLO-Methode*. Ph.D. thesis, Ruhr-Universität, Bochum, Germany, 1992.
(50) Lantto, P.; Vaara, J.; Helgaker, T. *J. Chem. Phys.* **2002**, *117*, 5998–6009.
(51) Kawamura, T.; Matsunami, T.; Yonezawa, T. *Bull. Chem. Soc. Jpn.* **1967**, *40*, 1111–1115.
(52) Griffith, O. H.; Dehlinger, P. J.; Van, S. P. *J. Membr. Biol.* **1974**, *15*, 159–192.
(53) Knauer, B. R.; Napier, J. J. *J. Am. Chem. Soc.* **1976**, *98*, 4395–4400.
(54) Stone, A. J. *Mol. Phys.* **1963**, *6*, 509–515.
(55) Stone, A. J. *Mol. Phys.* **1964**, *7*, 311–316.
(56) Aikens, C. M.; Fletcher, G. D.; Schmidt, M. W.; Gordon, M. S. *J. Chem. Phys.* **2006**, *124*, 014107.
(57) Röhrig, U. F.; Frank, I.; Hutter, J.; Laio, A.; VandeVondele, J.; Rothlisberger, U. *ChemPhysChem* **2003**, *4*, 1177–1182.
(58) Murugan, N. A.; Rinkevicius, Z.; Ågren, H. *J. Phys.Chem. A* **2009**, *113*, 4833–4839.
(59) de Almeida, K. J.; Murugan, N. A.; Rinkevicius, Z.; Hugosson, H. W.; Vahtras, O.; Ågren, H.; Cesar, A. *Phys. Chem. Chem. Phys.* **2009**, *11*, 508–519.
(60) Ahlström, P.; Wallqvist, A.; Engström, S.; Jönsson, B. *Mol. Phys.* **1989**, *68*, 563–581.
(61) Helgaker, T.; Jaszuński, M.; Ruud, K.; Górska, A. *Theor. Chem. Acc.* **1998**, *99*, 175–182.
(62) Schäfer,, A.; Huber, C.; Ahlrichs, R. *J. Chem. Phys.* **1994**, *100*, 5829–5835.
(63) Schmidt, M. W.; Baldridge, K. K.; Boatz, J. A.; Elbert, S. T.; Gordon, M. S.; Jensen, J. H.; Koseki, S.; Matsunaga, N.; Nguyen, K. A.; Su, S.; Windus, T. L.; Dupuis, M.; Montgomery, J. A. *J. Comput. Chem.* **1993**, *14*, 1347–1363.